Journal of Energy Chemistry 27 (2018) 146–160

Contents lists available at ScienceDirect

Journal of Energy Chemistry

journal homepage: www.elsevier.com/locate/jechem

http://www.journals.elsevier.com/journal-of-energy-chemistry/

Review

Nitrogen-doped graphene: Synthesis, characterizations and energy applications

Haifeng Xu[a,b,1], Lianbo Ma[a,1], Zhong Jin[a,*]

[a] Key Laboratory of Mesoscopic Chemistry of MOE, School of Chemistry and Chemical Engineering, Nanjing University, Nanjing 210023, Jiangsu, China
[b] School of Mechanical and Electronic Engineering, Suzhou University, Suzhou 234000, Anhui, China

ARTICLE INFO

Article history:
Received 21 November 2017
Revised 4 December 2017
Accepted 5 December 2017
Available online 9 December 2017

Keywords:
N-doped graphene
Synthesis
Characterization
Energy applications

ABSTRACT

Nitrogen-doped (N-doped) graphene has attracted increasing attentions because of the significantly enhanced properties in physic, chemistry, biology and material science, as compared with those of pristine graphene. By date, N-doped graphene has opened up an exciting new field in the science and technology of two-dimensional materials. From the viewpoints of chemistry and materials, this article presents an overview on the recent progress of N-doped graphene, including the typical synthesis methods, characterization techniques, and various applications in energy fields. The challenges and perspective of N-doped graphene are also discussed. We expect that this review will provide new insights into the further development and practical applications of N-doped graphene.

Haifeng Xu received his Ph.D. degree in Materials Science and Engineering from Anhui University (2015). He is an associate professor in School of Mechanical and Electronic Engineering at Suzhou University. He is now a visiting scholar in the research group of Prof. Zhong Jin at Nanjing University. His main interest is the fabrication of graphene-based materials for energy storage.

Lianbo Ma received his M.S. degree in Applied Chemistry from Jiangsu University (2015). He is now pursing his Ph.D. degree under the supervision of Prof. Zhong Jin in School of Chemistry and Chemical Engineering at Nanjing University. His main interests are the design and fabrication of nanomaterials for energy storage, electrochemistry, and photoelectric conversion.

Zhong Jin received his B.S. (2003) and Ph.D. (2008) in chemistry from Peking University. He worked as a postdoctoral scholar at Rice University and Massachusetts Institute of Technology. Now he is a professor in School of Chemistry and Chemical Engineering at Nanjing University. He leads a research group working on functional nanomaterials and devices for energy conversion and storage.

1. Introduction

Graphene, a two-dimensional (2D) sheet sp^2-hybridized carbon with special properties, such as planar structure, high surface area, excellent electrical and optical properties, and great mechanical properties (Young's modulus ~1.0 TPa and a fracture strength ~130 GPa) [1,2], has attracted so much attention since it was firstly exfoliated in experiment by Novoselov and Geim et al. [3,4]. During the last decade, great efforts were devoted to investigate the possible applications of graphene based on those above excellent properties. For example, hollow Pt-Ni decorated on graphene was fabricated, and the resultant composite exhibited much higher electrocatalytic activity as compared with bare Pt-Ni catalyst, owning to the significantly enhanced electrical conductivity and reduced particle aggregations [5]. Pt/graphene [6], Fe_3O_4/graphene [7], CoSe/graphene [8], and PtRuNi/graphene [9] were also synthesized, and all of them show the obviously improved performances.

* Corresponding author.
E-mail address: zhongjin@nju.edu.cn (Z. Jin).
[1] Both authors contributed equally to this work.

https://doi.org/10.1016/j.jechem.2017.12.006

The structures and properties of carbonaceous materials can be effectively tailored by heteroatoms doping. Following this line of thought, doping nitrogen (N) atoms into graphene can significantly affect the properties and performance of graphene-based materials. Peng et al. firstly reported the fabrication of nitrogen-doped (N-doped) graphene, and adopted it as the electrocatalysts in oxygen reduction reaction (ORR) [10]. It was revealed that the N-doped graphene exhibits superior electrocatalytic activity than most of other electrocatalysts. This has attracted great attention and further made N-doped graphene a hot topic. Just from that time, N-doped graphene developed rapidly. By date, many synthesis methods, including chemical vapor deposition (CVD) [11–20], thermal annealing [21–36], pyrolysis [37–41], arc-discharge [42–44], plasma treatment [45–47], N_2H_4 treatment [48–50], hydrothermal method [51–54], solvothermal method [55–58], microwave-assisted hydrothermal [59–61], wet chemical synthesis [62], microwave treatment [63], flame treatment [64], supercritical reaction method [65] and lyophilization-assisted heat treatment [66], have been exploited to prepare N-doped graphene. Graphene sheets doped with N atoms would generate three kinds of common bonding configurations within the lattice, including pyridinic N, graphitic N and pyrrolic N [67]. Among them, the mostly widely discussed was pyridinic N and pyrrolic N. Luo et al. reported the synthesis of single layer graphene doped with pure pyridinic N by thermal CVD of hydrogen and ethylene on Cu foils in the presence of ammonia [68]. Such pyridinic N doping in carbon materials was generally considered to be responsible for their enhancement of ORR activities. Zhang et al. synthesized the N-doped graphene through the thermal annealing method [69], and the resultant material shows a higher electrochemical activity towards methanol oxidation than Pt. These results demonstrated that N doping can really enhance the properties of graphene as compared with those of pristine graphene. Because of the intriguing structures and properties, N-doped graphene has been widely used in the fields of electronics [70], fuel cells [71], secondary batteries [72–74], supercapacitors [75,76], medical domain [77], and so on, and most of the materials can satisfy the expectations.

Recently, several reviews on graphene and graphene-based materials have been reported [1,78]. However, to the best known of our knowledge, a review of N-doped graphene includes the synthesis methods, characterization techniques, energy applications, as well as challenges and perspectives, is still emergently needed. From the viewpoints of chemistry and materials, this article will present an overview on the recent progress of N-doped graphene.

2. Preparation of N-doped graphene

The first employed methods for preparing N-doped graphene usually including chemical vapor deposition (CVD) and arc-discharge method, which were reported by Wei et al. [12] and Subrahmanyam et al. [79], respectively. Currently, there are many synthesis methods explored during such a short time. Table 1 summarizes the various methods for preparing N-doped graphene. The N contents, experimental details, applications and advantages for the synthesis/applications of N-doped graphene are also involved. Moreover, we have divided the synthesis methods into the one-step N doping and two-step N doping strategies. The one-step N doping strategy commonly include CVD, flame treatment and solvothermal method, while the two-step N doping strategy mainly include thermal annealing, pyrolysis, N_2H_4 treatment, wet chemical synthesis, microwave treatment, supercritical reaction, hydrothermal method, microwave-assisted hydrothermal method and lyophilization-assisted heat treatment. Detailed discussions on these methods are followed below.

2.1. CVD

CVD is one of the mostly used methods for preparing N-doped graphene [11–20], and it usually includes two precursors, N precursor and graphene precursor. The commonly adopted N precursor was NH_3 [11–14]. However, besides the gas phase precursor, pyridine and polypyrrole were also employed with the presence of carrier gases [15,16,19].

The synthesis procedures usually include the following essentials: first of all, a metal catalyst, like Ni and Cu, and a Si/SiO_2 plate, used as the substrate [11,13,17]. Then, a mixed gas containing carbon precursor and N precursor were introduced with the temperature increasing to a high position [17]. The C and N precursors decomposed and recombined into a new structure that looks like the graphene sheets on the substrate. Therefore, N-doped graphene can be prepared, as schematic illustrated in Fig. 1. The resultant morphology observation shows that most of the structure composed of few layers of graphene monomer, although single layer graphene could be occasionally detected [12].

The mechanism of this method can be postulated that graphene grew on the substrate and N atoms substitutionally doped into the graphene lattice. By incorporating N atoms into graphene, the physic and chemical properties of pristine graphene could be significantly altered [17]. The N contents of this method commonly various from 3.0 to 16 at.%. Moreover, it was reported that the influence factors of CVD includes gas ratio of mixture [12], and deposition conditions [13]. The reported highest N content by using CVD was 16.7 at.% [15], while the lowest N content was 0.25 at.% [17]. Additionally, the N content in N-doped graphene is a very important factor that influences the type of N atoms in graphene. The pyridinic N structure becomes favorable as the N content increases, which plays a key role on the enhancement of electrocatalytic activity and energy storage performance [13].

2.2. Thermal annealing

Thermal annealing is a popular method in the preparation of N-doped graphene owning to the simple and scalable characteristics. The N doping can be achieved through annealing graphene oxide (GO) under NH_3 atmosphere at a comparable high temperature [21–36]. Different temperatures would lead to different N contents as well as the diversity in performance activities [21,23]. The N contents of N-doped graphene prepared through this method usually range from 1.1 to 7.5 at.%.

Besides NH_3, other materials with high N contents were also used as the N precursors. For instance, GO annealed with urea can produce N-doped graphene [30], and the N content could reach as high as 10 at.%. The N content of this method depends mostly on the N content of N precursor. Sometimes, N doping also accompanied with other heteroatoms, such as sulfur and boron atoms, and the resultant products could show synergy effects between the N atoms and other heteroatoms [26,32].

2.3. Pyrolysis

Pyrolysis usually operated under a higher temperature than thermal annealing [37–41]. The pyrolysis of GO and N-containing precursors is a promising method for preparing N-doped reduced GO (rGO). The most extensively used N precursors were polyaniline [37], melamine [38,40,41], and polypyrrole [39]. The common process usually consisted of two steps, the combination between GO and N precursor and followed with pyrolysis of the as-formed composites. This method prone to produce a medium high N content that range from 2.0 to 8.0 at.%. As N-doped porous carbon materials prepared though pyrolysis of ethylenediaminetetraacetic

Table 1. Summary of the synthesis methods, N contents, applications and advantages in synthesis/applications of N-doped graphene.

Synthesis methods	Substrate N/C sources	N content (at.%)	Applications	Advantages in synthesis/applications	Ref.
CVD	Ni on SiO_2/Si substrate CH_4/NH_3	4.0	Fuel cell	Enhanced ORR activity	[11]
CVD	Cu on Si substrate CH_4/NH_3	8.9	Semiconductor device	Excellent electronic properties	[12]
CVD	Si nanowire substrate CH_4/NH_3	3.0–10	Li-ion battery	Controlled thickness, N content and enhanced lithium storage capability	[13,14]
CVD	Cu foil substrate pyridine	16.7/~2.4	Electronic devices	Controlled thickness, high electronic mobility and low temperature	[15,16]
CVD	Cu foil substrate CH_4/NH_3	0.25	Molecule probe	Enhanced molecule sensing	[17]
CVD	Cu foil substrate DMF	3.4	Electronic devices	Controlled thickness	[18]
CVD	Cu foil substrate polypyrrole	–	FET-type Apta sensor	Well controlled growth	[19]
CVD	Cu foil substrate hexane acetonitrile	9.0	Li-ion battery	Enhanced lithium storage capacity	[20]
Thermal annealing	GO/NH_3	4.0–7.0	Optics/fuel cell/clean energy	Tunable optical properties, high electrochemical activity	[21–24]
Thermal annealing	Mn_3O_4/GO/NH_3	1.13	Li-ion battery	Large reversible capacity, excellent cyclic performance	[25]
Thermal annealing	GO-Si sheet/NH_3	2.4–4.6	Fuel cell	Enhanced electrocatalytic properties	[26]
Thermal annealing	GO/NH_3/Ar	3.63–7.45	Li-ion battery/ supercapacitor	Tunable structure, improved electrochemical performance	[27–29]
Thermal annealing	GO/NH_3/CdS	4.3	Photocatalysis	High durability, enhanced photocatalytic activity	[30]
Thermal annealing	NH_3 annealing after N^+ irradiation of graphene	1.1	Semiconductor device	Excellent electronic properties	[31]
Thermal annealing	GO/boric acid/NH_3	–	Fuel cell	Efficient electrocatalytic ORR activity	[32]
Thermal annealing	GO/melamine/Ar	10	Electronic device	Graphene structure can be controlled	[33]
Thermal annealing	[TPBAIm][*NTf*2], carbonization with N_2	4.45–7.15	Domino carbonylation	One-pot synthesis, facile and novel method	[34]
Thermal annealing	GO/NH_3/Ar	2.8	–	Enhanced conductivity	[35]
Thermal annealing	GO/urea	4.0	Fuel cell	High electrocatalytic activity in ORR	[36]
Pyrolysis	rGO/polyaniline	4.82–5.86	Fuel cell	High electrocatalytic activity in ORR	[37]
Pyrolysis	Aniline/melamine/$FeCl_3$	–	Fuel cell	Excellent electrocatalytic activity in ORR	[38]
Pyrolysis	GO/polypyrrole	2.0–3.0	Fuel cell	High electrocatalytic activity in ORR and OER	[39]
Pyrolysis	GO/melamine	3.7	Fuel cell	High specific area and good crystallinity	[40,41]
Arc-discharge	Graphite powder/N_2	<1.0	–	Safe, simple and inexpensive	[42]
Arc-discharge	Graphite anode NH_3/H_2/He	1.0	Field effect transistor	Highest mobility, smallest number of layers	[43]
Arc-discharge	Graphite anode NH_3/He	1.0	–	Large-scale produced and controllable	[44]
Plasma treatment	N_2 plasma/graphene	0.11–1.35	Glucose sensor	Excellent electrocatalytic activity and selectivity	[45]
Plasma treatment	Si substrate CH_4/N_2 (1: 4) plasma	0.7–6.3	Field emitter	Lower turn-on field and enhanced current density	[46]
Plasma treatment	GO/N_2 plasma treatment	1.68–2.51	Supercapacitor	High capacitance and excellent cycle life	[47]
N_2H_4 treatment	GO/N_2H_4 for 1 h and reduced by NH_3/H_2	7.3	Poly(light emitting diodes)	Lowest sheet resistance	[48]
N_2H_4 treatment	GO/NH_4OH mixture reduced by N_2H_4	8.92	Electrochemical sensor	Favorable electron transfer ability and electrocatalytic activity	[49]
N_2H_4 treatment	GO/N_2H_4	2.7–3.2	Rewritable nonvolatile memory materials	High semi-conductivity	[50]
Hydrothermal	GO/NH_4OH (28 wt.%)	7.2	Supercapacitor	Excellent thermal stability, high capacitive performance	[51]
Hydrothermal	GO/urea	10.13	Supercapacitor	Large surface area, superior capacitive performance	[52]
Hydrothermal	Graphite oxide/ammonium vanadate	–	Li-ion battery	High rate capability, excellent conductivity and cyclic stability	[53]
Hydrothermal	GO/polypyrrole/iron ions	3.5	Fuel cell	High specific area, high durability	[54]
Solvothermal	Li_3N/CCl_4/Ar, 200 °C, 20 h (N1) $Li_3N/CCl_4/N_2$, 250 °C, 10 h (N2)	10.5 (N1)/ 4.15–16.4 (N2)	Fuel cell	High electrocatalytic activity in ORR	[55,56]
Solvothermal	Li_3N/CCl_4 with $N_3C_3Cl_3$ (350 °C,6 h, N1) or (250 °C, 10 h, N2)	16.4(N1)/4.5(N2)	Fuel cell	High electrocatalytic activity in ORR	[57]
Solvothermal	Tetrachloroethylene /cyanuric chloride	28.1	H_2 storage	High H_2 physisorption capacity	[58]
Microwave-assisted hydrothermal	GO/urea	3.0	Fuel cell	High capacity, enhanced electronic properties	[59]
Microwave-assisted hydrothermal	GO/NH_4OH	< 1.0	Supercapacitor	Enhanced energy and power density	[60]
Microwave-assisted hydrothermal	GO/ethylenediamne	1.98	Li-ion battery	Super energy storage performance	[61]
Wet chemical synthesis	GO/dicyandiamide/Fe^{3+}	–	Fuel cell	High electrocatalytic activity in ORR	[62]
Microwave treatment	GO/$NH_3/H_2PtCl_6 \cdot 6H_2O$	5.04	Fuel cell	High electrocatalytic active surface area	[63]
Flame treatment	Ethanol (70%) /$NH_3 \cdot H_2O$ (30%)	1.4	Supercapacitor/catalysts	Abundant surface defect, high catalytic activity	[64]
Supercritical reaction method	Expanded graphite/acetonitrile	1.57–4.56	Nanoelectronic device	Modulated electrical properties	[65]
Lyophilization-assisted heat treatment	Graphite oxide/urea	5.06	Fuel cell	Enhanced electrocatalytic activity and stability in ORR	[66]

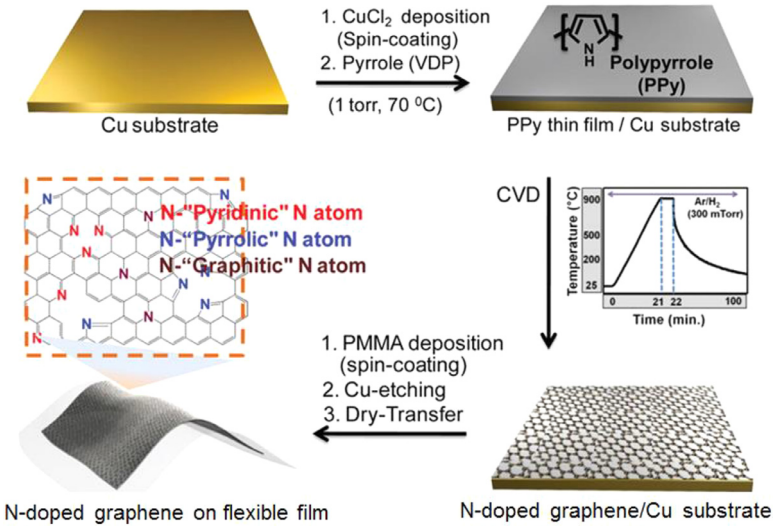

Fig. 1. Schematic illustration of the synthesis of N-doped graphene on flexible substrate [19].

acid and melamine show a high N content (10.8 at.%) [80], more attentions would be paid to this method.

2.4. Arc-discharge method

Arc-discharge is an old fashioned method for preparing N-doped graphene. It usually includes N_2 or a gas mixture as the N sources [42–44]. This method always composed of two electrodes, and both of them were graphite rods, then a current was held. As the rods were brought together, discharge occurred, resulting in the formation of plasma. The anode was vaporized in NH_3 included mixing atmosphere or pure N_2 atmosphere. Li et al. synthesized N-doped graphene via arc-discharge method with NH_3 and He gas mixture as the N source [44]. The N content of this method was lower as compared with other methods, and it usually belows 1.0 at.% [42].

Large-scale N-doped multi-layered graphene can be prepared by using the direct current arc-discharge between pure graphite rods [44]. During this method, NH_3 was used as the buffer gas, and the multi-layered graphene sheets were doped with N atoms without the addition of other N sources. The N content in the N-doped multi-layered graphene sheets was low, but it can be tuned by simply changing the proportion of NH_3 in the mixed gas. This technique curves a way in large scale production of N-doped graphene sheets without the use of any metallic catalyst, which is crucial to the further study and applications.

2.5. Plasma treatment

Plasma treatment is a technique that invented to produce N-doped graphene several years ago [45–47]. However, few attentions have been paid to this method, and there was no notable progress obtained till now. Wang et al. used N_2 plasma as the N source, and then reacted with graphene to prepare N-doped graphene [45]. In the first place, graphene was fixed onto glass carbon electrode (GCE), followed by placing it into the plasma chamber that filled with N_2 with the pressure at 750 mTorr. In other reports, graphene was not used, but CH_4 acted as the carbon source [46], thus the N-doped graphene was prepared on the Si substrate directly. The schematic illustration of the plasma doping process is shown in Fig. 2. All the reports that related to N content are very low, which usually below 3.0 at.% [47]. Therefore, the method would have its limitation on the N content, as well as the properties and applications.

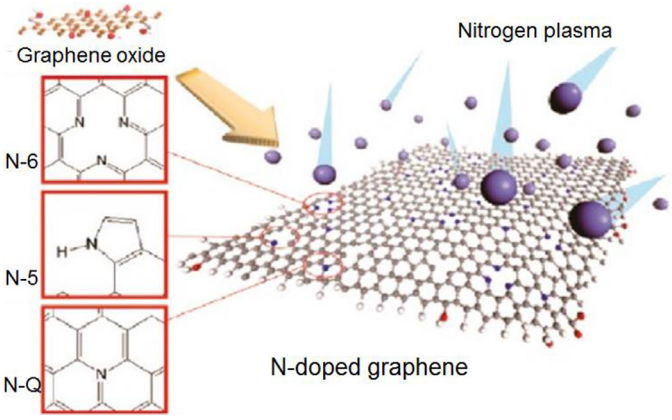

Fig. 2. Schematic illustration of the plasma doping process of N atoms on graphene sheets [47].

2.6. N_2H_4 treatment

N_2H_4 treatment is one of the widely used methods for preparing N-doped graphene from GO [48–50], and N_2H_4 usually serves as the reducing agent during the reaction [81]. N_2H_4 solution was the commonly used state in the method. However, it was reported that N-doped graphene could also be synthesized by using N_2H_4 vapor when the temperature is above 750 °C [48]. The N content of N-doped graphene can be up to 7.2 at.%. Sohyeon et al. also reported that N-doped graphene could be prepared by using NH_4OH and N_2H_4 mixed solution, and the N content would be higher than the former, which can reach about 8.92 at.% [49]. The N types always include pyridinic N and pyrrolic N, both are very important to the properties and applications of N-doped graphene.

2.7. Hydrothermal method

Hydrothermal method for preparing N-doped graphene is very popular in recent years, and there are many reports about it [51–54]. By mixing GO and different N precursors together, N-doped graphene with various N contents were obtained. It was reported that GO dispersed into ammonia solution and then heated in an autoclave with different temperatures, N-doped graphene with varies N contents could be produced [54]. The other methods with different N precursors, such as polypyrrole and urea, were also suc-

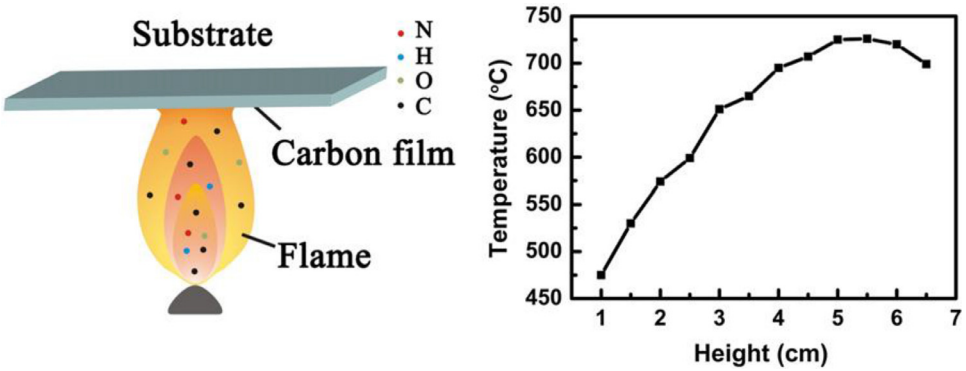

Fig. 3. Diagram of the flame treatment and the corresponding temperature profile [64].

cessful in synthesizing N-doped graphene [52,54]. When urea was served as the N precursor, the resultant product exhibits a highest N content of 10.13 at.% [52]. Because of its simple procedure and the high N content, hydrothermal method would be a promising method in preparing N-doped graphene.

2.8. Solvothermal method

The solvothermal method was used to prepare N-doped graphene since several years ago [55–58]. All of the reports seemed to have no big difference from each other. The common procedure was mixing tetrachloromethane (CCl_4) and lithium nitride (Li_3N) together, followed by reacting in a sealed stainless steel autoclave under Ar atmosphere [55]. The other method was mixed tetrachloromethane (CCl_4) and lithium nitride (Li_3N) together with cyanuric chloride ($N_3C_3Cl_3$), followed by reacting in stainless steel autoclave in N_2 atmosphere [57]. The results concluded that N-doped graphene prepared via this method can be developed as an efficient electrocatalyst for ORR, and can be used to replace the precious Pt catalysts in alkaline solutions. The N contents of N-doped graphene prepared through this method was estimated range from 4.0 to 28.1 at.%.

2.9. Microwave-assisted hydrothermal method

Microwave-assisted hydrothermal is a new method that reported recently [59–61]. Graphite oxide combined with a N precursor under the microwave treatment, followed by the hydrothermal treatment, N-doped graphene can be well synthesized. The commonly used N precursors in this method includes urea [59], NH_4OH [60], and ethylenediamne [61], the N content of this method was about 3.0 at.%.

2.10. Wet chemical reaction method

Recently, a method for preparing N-doped graphene without high temperature treatment was reported, which called wet chemical reaction method [62]. It was proposed that the reaction occurred between a reactive graphitic carbon template (e.g. GO) and N-containing molecules (e.g. dicyandiamide), when the temperature is as low as 180 °C. The process of this method includes several sophisticated steps. It was believed that the wet chemical reactions may offer a low-temperature route to create interesting electrocatalysts in fuel cells with easier manipulation of surface properties [62].

2.11. Microwave method

The microwave method was firstly reported in 2011, and has been proved to be successful in preparing N-doped graphene [63]. N-doped graphene was prepared from GO via microwave heating in NH_3 atmosphere. The results showed that graphene, as an allotrope of carbon, is a good microwave-adsorbing material and can reach a high temperature in minutes, facilitating N incorporation into the structure under NH_3. The structural characterizations demonstrated that the N content can reach 5.04 at.%. Other efforts on this method were also reported recently. For example, Yoo et al. synthesized the highly wrinkled N-doped rGO through direct microwave irradiation from graphite oxide and aqueous ammonium hydroxide (NH_4OH) in only three minutes, and the resultant material exhibited superior capacitive performance and electrocatalytic activity [82].

2.12. Flame treatment

Flame treatment is a novel method that firstly used in 2012 [64]. The schematic illustration of flame treatment is shown in Fig. 3. This is a really simple but effective method for preparing N-doped graphene. During the synthesis process, ethanol and amine were used as the C and N precursor, respectively, a Ni film was selected as the catalyst for growing graphene, when amine and ethanol were used as fuel, the N-doped graphene would be obtained only with the temperature higher than 700 °C. The achieved results revealed that graphene sheet from flame treatment exhibits good transparency and a large size up to 400 um^2 with few layers and folded edges. These results also informed that N-doped graphene sheets have a dominant pyridinic N structure. Moreover, N-doped graphene prepared by this method can be used as a promising candidate for supercapacitors and catalysts, owning to much more structural defects induced by the environment conditions and N atoms.

2.13. Supercritical reaction method

The supercritical reaction method was firstly reported in 2011, and it is really a difficult method because of its complicate conditions during the reactions [65]. The schematic illustration of N-doped graphene sheets prepared via supercritical reaction method is shown in Fig. 4. N-doped few-layer graphene was prepared via this method, and the N contents increased from 1.57 to 4.56 at.% as the reaction time tuned from 2 to 24 h. Electrical measurements revealed that N-doped few-layer graphene sheets exhibit a typical n-type field-dependent behavior, further suggesting that the N atoms have been doped into the lattice of graphene.

2.14. Lyophilization-assisted heat treatment

Lyophilization-assisted heat treatment is a method of heat treatment combined with lyophilization technology. This method

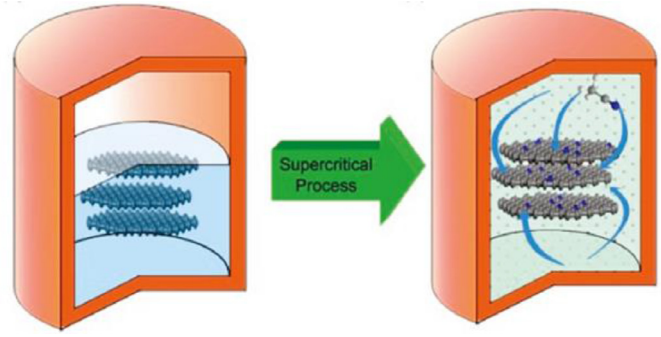

Fig. 4. Schematic illustration of N-doped graphene sheets prepared via supercritical reaction method with acetonitrile (ACN) at 310 °C [65].

is similar to the microwave-assisted hydrothermal method. The N content of achieved N-doped graphene can be as high as 5.06 at.%, and pyridinic N was the dominant N species through this intriguing method [66].

3. Characterizations of N-doped graphene

3.1. Scanning tunneling microscopy (STM)

STM is very useful for imaging material surfaces at the atomic level, and is considered as one of the most powerful techniques for characterizing N-doped graphene. This tool is so direct that we can see the atomic details of the N-dopants in N-doped graphene. However, although STM simulation of N-doped graphene has been widely investigated [83,84], the experimental studies on STM characterization on N-doped graphene have been rarely reported. Fig. 5 shows the STM image of typical N-doped graphene that prepared through atmospheric-pressure CVD method by Terrones and his coworkers [17]. The STM measurement was usually performed after transferring N-doped graphene onto other substrates because the Cu foil could affect STM imaging due to the charging screening in the graphene layer. The STM images show a rough surface with a corrugation of 0.6–1.0 nm, which could be attributed to the roughness of the substrate. The representative STM topographic image of N-doped graphene reveals the clear honeycomb lattice mostly decorated with brighter "peapod-like graphic protrusions", as pointed by the white arrows in Fig. 5(a). Since similar features were observed all over the N-doped graphene surface and were never detected in pristine graphene, thus it can be deduced that the specific features are caused by the presence of N-dopants [17]. Fig. 5(b) and (c) show the experimental results and simulated highly resolved STM images of an individual N-doped site, the overall triangular shape and mirror plane of the calculated STM images are in good agreement with the experimental results. Similarly, the information of N-dopants can also be achieved from the N-doped graphene sheets that prepared by the solvothermal method [56].

3.2. X-ray diffraction (XRD) characterization

XRD pattern is the widely used method to distinguish the compositions and crystallinity of the as-prepared materials. Fig. 6 presents the XRD patterns of graphite, GO, and N-doped rGO

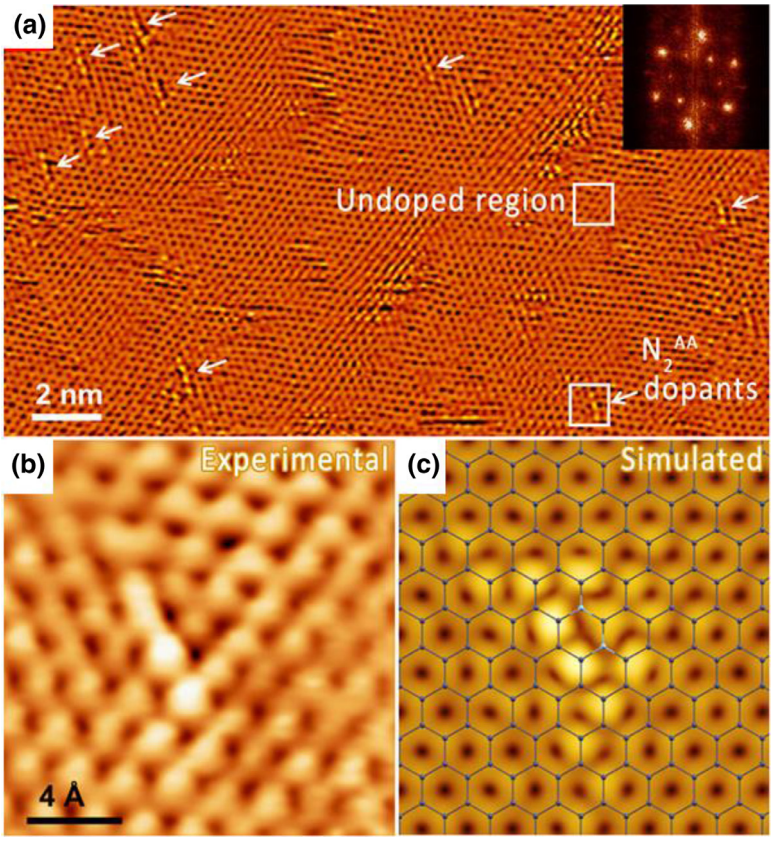

Fig. 5. (a) Large-area STM image of N-doped graphene illustrating the presence of numerous N-dopants with similar peapod-like configuration (highlighted by white arrows), $V_{bias} = -75$ mV, $I_{set} = 100$ pA. The upper and lower squares are used to indicate the undoped region and N-dopants. The inset shows the FFT pattern of topography presents reciprocal lattice (outer hexagon) and inter-valley scattering (inner hexagon). The STM image shown here is obtained with flattening mode to remove the overall roughness of the substrate and enhance the atomic contrast of dopants. (b) High-resolution STM image of a N-doped site. (c) Ball-stick structural model of the N-doped site and a simulated STM image obtained using first-principle calculation. The bias is 21.0 eV. The C and N atoms are illustrated using gray and cyan balls, respectively [17].

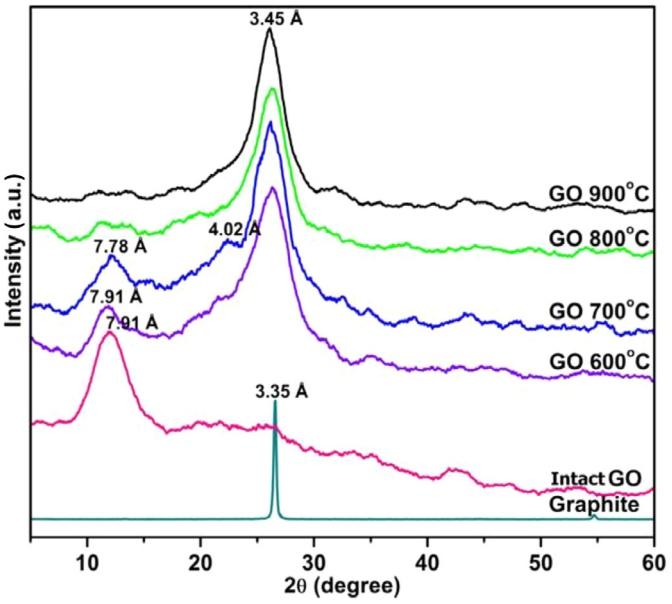

Fig. 6. XRD patterns of graphite, GO, and N-doped rGO prepared by annealing GO under various temperatures in Ar/NH_3 atmosphere, respectively [27].

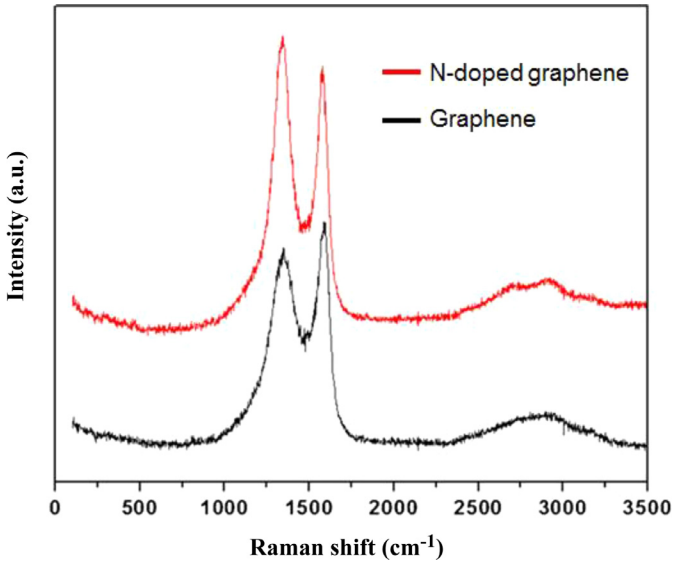

Fig. 7. Raman spectra of N-doped graphene and graphene [35].

prepared by annealing GO under various temperatures in mixed Ar/NH_3 atmosphere. It could be concluded from the XRD results that the interlayer distance of graphite was 3.35 Å, while the interlayer distance of intact GO turned to be 7.91 Å due to the sufficient oxidation and inter-laminar water [27]. After the reduction of GO in Ar/NH_3 under high temperatures from 600 to 900 °C, the interlayer distance of N-doped rGO decreases gradually. This may be because the interlayer distance between oxygens in N-doped rGO at high temperatures are around 7.78–7.91 Å and the interlayer distance between carbons in N-doped graphene are around 3.35 Å. With the increase of temperature, the oxygen-rich regions would be significantly decreased. Moreover, the peak intensities of oxygen-rich regions in N-doped rGO at high temperatures are lower than those at low temperatures, which can also be ascribed to the decreased oxygen-rich regions at high temperatures. Li et al. reported that N-doping is accompanied with the reduction of GO with decreases in oxygen levels from about 28% in as-made GO down to about 2.0% in NH_3 reacted GO at 1100 °C [23]. The diffraction peak located at $2\theta = 11.5°$ was attributed to the (002) crystalline plane of GO, while Sun et al. reported it at $2\theta = 10.1°$, which was synthesized through hydrothermal method [52]. The same phenomenon between these two reports is that the diffraction peak disappeared when the reaction temperature increased to a much higher degree. The diffraction peak at $2\theta = 25°$ with high temperature indicates that the framework of reduced sample is composed of few-layer stacked graphene nanosheets [85].

3.3. Raman spectroscopy

Raman spectroscopy is a spectroscopic technique for observing the vibrational, rotational, and other low-frequency modes of molecules, and is commonly used in chemistry to provide a structural fingerprint by which different materials can be identified. Fig. 7 shows the typical Raman spectra of N-doped graphene and graphene; two distinct peaks and a weak peak are observed. The peak located at approximately 1340 cm^{-1} is attributed to D band, while Guan et al. [42] and Li et al. [44] reported that it located at about 1289 cm^{-1} and 1350 cm^{-1}, respectively. The G band, at approximately 1570 cm^{-1}, is commonly observed in all graphitic structures. The difference between N-doped graphene and pristine graphene was mentioned by Wang's group [11], which revealed that G band of N-doped graphene was located at 1576–1582 cm^{-1}, while for the pristine graphene, produced by CVD, the G band was centered at 1583–1588 cm^{-1}. The weak peak belongs to the 2D band, and it is the overtone of D band. The 2D band is always observed in carbon materials [86]. However, the most important is that the intensity of 2D band is sensitive to the number of graphene layers [42]. The location of 2D band is also different in N-doped graphene that previously reported [12,20,31,42,44].

3.4. X-ray photoelectron spectroscope (XPS) characterization

XPS is a surface-sensitive quantitative spectroscopic technique that can reveal the elemental compositions, empirical formula, chemical states and electronic states of the elements that exist within a material [87]. By analyzing the binding energy (B_E) values, we can confirm the nature of the bindings between C and N [39]. Fig. 8(a) compares the typical survey XPS spectra of N-doped graphene and pristine graphene, a distinct peak at approximately 400 eV shows the N 1*s* band of the N-doped graphene. Moreover, the N content in N-doped graphene can be directly achieved from the XPS analysis. It should be emphasized that no signal related to N could be detected from the survey XPS spectrum of pristine graphene [18]. N 1*s* peak is the typical feature of N-doped graphene. Qu et al. [11], Wei et al. [12], and Yong et al. [13] reported the peak position at 400 eV, 401.6 eV, and 400.5 eV, respectively. Moreover, the devolution of high-resolution XPS spectrum at N 1*s* region yield three kinds of N functional groups (Fig. 8b): pyridinic N, pyrrolic N, and graphitic N, which centered at 398.3 eV, 399.4 eV, and 401.1 eV, respectively [22,24]. Among the above three N types, only pyrrolic N is known to improve the electrical conductivity of graphene films [88]. Pyridinic N with a localized one pair of electrons inevitably accompanies a vacancy defect. Graphitic N is usually present at N-containing dangling bonds or physic-sorbed species that cannot contribute to the recovery of hexagonal graphitic structure [48]. However, pyrrolic N is known to maintain a sp^2-hybridized graphitic structure as well as to improve the electrical conductivity by providing delocalized electrons [89]. These results further confirm the successful chemical doping of N into graphene structure [24]. The percentage of these three kinds of N atoms can also be known through calculating the area of each type of N species [27].

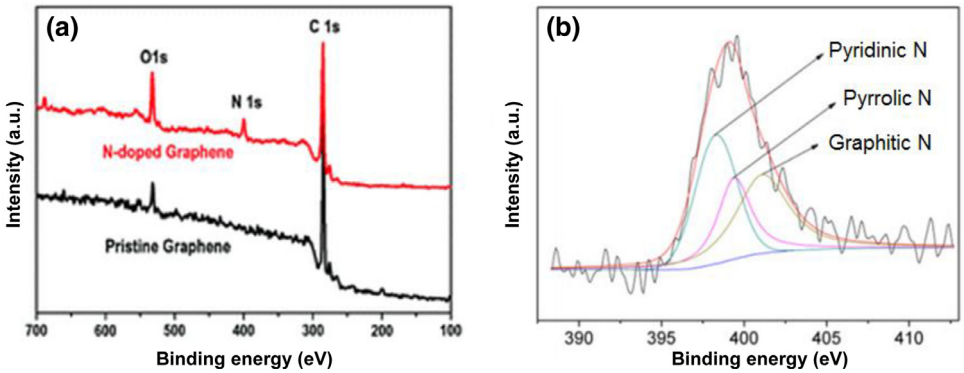

Fig. 8. (a) XPS spectra of N-doped graphene and pristine graphene [12]. (b) High-resolution XPS spectrum at N 1*s* region of N-doped graphene [24].

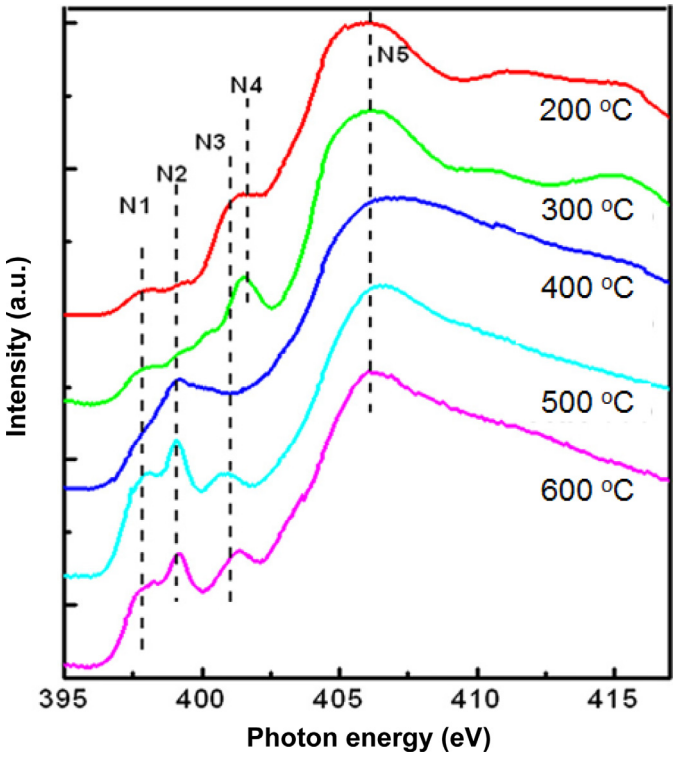

Fig. 9. Comparisons of the N K-edge XANES spectra of N-doped graphene prepared by annealing GO/urea mixture under different temperatures (200, 300, 400, 500 and 600 °C) [33].

Besides the information above, the spectra of C 1*s* and N 1*s*, which not provided here, can also be deconvoluted into several components. Devolution of C 1*s* always included C–N (285.9 eV), C–C (284.5 eV), C–O (286.5 eV), C=O (287.9 eV), and O–C=O (289.1 eV) [24]. While the devolution of O 1*s* contained O–C band at 531.5eV, O=C band at 532.6 eV, and O–C=O band at 533.8 eV, respectively [22].

3.5. X-ray absorption of near-edge structure (XANES) characterization

XANES is a type of absorption spectroscopy that indicates the features in the X-ray absorption spectra of condensed matter. Recently, XANES were performed to characterize the N-doped graphene [33,35]. However, as demonstrated in Fig. 9, the most representative sample is the characterization of N-doped graphene that prepared via thermal annealing at different temperatures. During the experiments, XANES would produce three kinds of K-edge XANES spectra, which includes C K-edge XANES spectra, N K-edge XANES spectra, and O K-edge XANES spectra.

Fig. 9 shows the comparison of N K-edge XANES spectra for the N-doped graphene. Position at about 406 eV (N5) in the sample that treated at 200 °C is ascribed to the σ^* excitation of C–N bonds [90,91], while Geng et al. reported it at about 406.3 eV [35]. A feature about 402 eV (N4) is observed, and it can be attributed to the attachment of urea species [33]. What is more, amino induced small features at about 399 eV (N1 and N2) can also be observed [92]. Because of a reduction of urea specie, decreased N4 peak is observed while the temperature increasing to 300 °C. As the temperature increases to 400 °C, a strong feature N2 emerges accompanied with the disappearance of the N4 peak. The disappearance of N4 peak can be deduced to the removal of urea species [89]. When the temperature reaches 500 °C, the intensities of N1 and N3 increase, and on the contrary, the intensity of N4 peak decreases. The N1 and N3 can be ascribed to pyridinic type and graphitic type doping of N species, respectively [89,90].

When the temperature increases to 600 °C, similar phenomenon can be observed, the graphitic N specie would be the dominant type with the N3 peak increases greatly [89,91]. It can be concluded that the pyridinic and graphitic N species occurred at the very high temperature [33].

C and O K-edge XANES spectra can also give some information about the structure, for instance, the C K-edge will clearly exhibit a π^* and a σ^* resonance and the effect of N-doping on the content of oxygen-containing groups in graphene can be confirmed by the comparison of O k-edge XANES spectra [35].

3.6. Other characterization techniques

Besides the typical tools mentioned above, other characterization techniques, such as atomic force microscope (AFM) [18,19,26,27,51], scanning photoelectron microscope (SPEM) [47], electron energy lose spectra (EELS) [14], thermogravimetric analysis (TGA) [44,62], infrared spectra (IR) [27,35,41], N_2 adsorption/desorption isotherm [39,40,52], energy dispersive spectrum (EDX) [24], selected area electron diffraction (SAED) [47], and bright field STEM (BF-STEM) [51,53], have also been employed to characterize N-doped graphene. Among them, SAED pattern as well as SPEM image can show the original layered structure and honeycomb-like atomic structure of graphene. AFM can be used to estimate the thickness of graphene, furthermore, the number of graphene layer. Moreover, EELS spectra can demonstrate the N contents in the N-doped graphene layer.

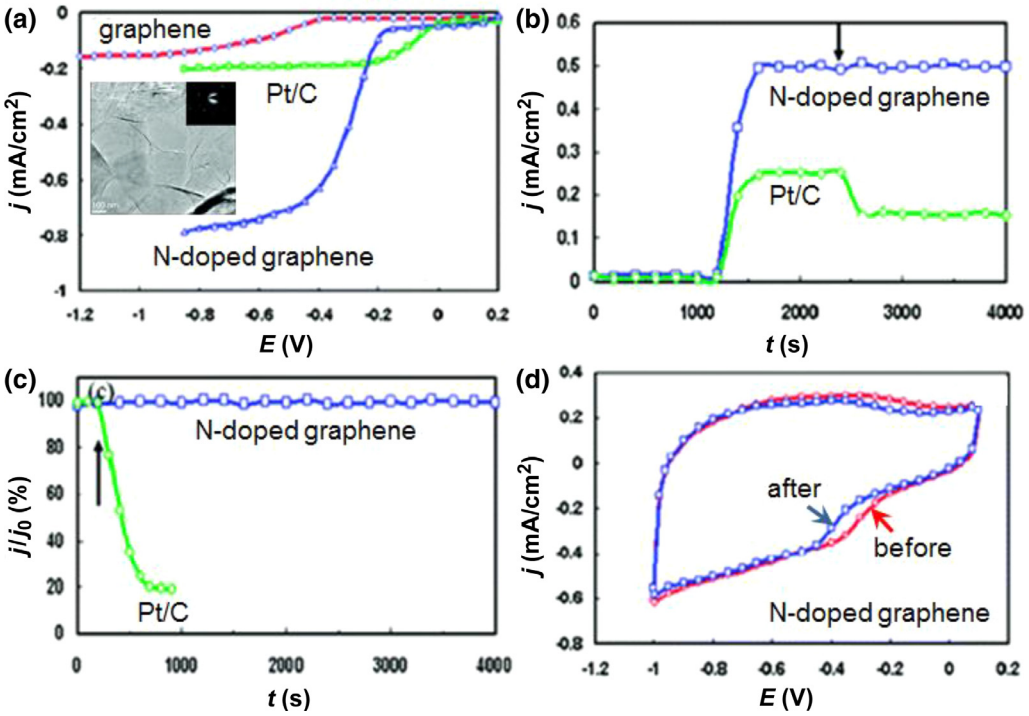

Fig. 10. Electrocatalytic activity comparisons of N-doped graphene and Pt/C. (a) RRDE voltammograms for the ORR in air-saturated 0.1 M KOH at the N-doped graphene, Pt/C, and graphene electrodes. Electrode rotating rate: 1000 rpm. Scan rate: 0.01 V s^{-1}. $Mass_{(graphene)} = Mass_{(PtC)} = Mass_{(N\text{-}doped\ grapene)}$ = 7.5 μg. The inset of (a) shows the typical morphology of N-doped graphene. (b) Current density (j)–time (t) chronoamperometric responses obtained at the N-doped graphene and Pt/C electrodes at −0.4 V in air-saturated 0.1 M KOH. The arrow indicates the addition of 2% (w/w) methanol into the air-saturated electrochemical cell. (c) j-t chronoamperometric response of N-doped graphene and Pt/C electrodes to CO. The arrow indicates the addition of 10% (v/v) CO into air saturated 0.1 M KOH at −0.4 V; j_0 defines the initial current. (d) Cyclic voltammograms of N-doped graphene electrode in air saturated 0.1M KOH before and after a continuous potentiodynamic swept for 200,000 cycles at room temperature (25 °C). Scan rate: 0.1 V s^{-1} [11].

4. Applications

N-doped graphene can exhibit significantly improved performances in various applications as compared to pristine graphene, including electrocatalytic activity [36,45,49], energy storage [25,28], transport properties [93], and other fields [19,45,48-50,65,94], owning to the modifications in structure and morphology. However, besides the bare N-doped graphene, N-doped graphene supported Pt [24,35, 63,64,95], Pd [34], FeCo [37], Fe_3O_4 [54], Mn_3O_4 [60], Zn_2GeO_4 [61], SnO_2 [96], CeO_2 [97], FeCo@carbon [98], and other inorganic materials were also reported. In the following, we will summary several applications of N-doped graphene in energy fields.

4.1. Electrocatalysts in fuel cells

Electrocatalysts play a key role in the performances of fuel cells. Noble metals, including Pt and Pd, were used as the electrocatalysts. However, their scarce nature limits the extensive applications in fuel cells, thus to find an ideal electrocatalyst for replacing the noble metals is emergently needed. Graphene is an excellent candidate, and it can exhibit much better electrocatalytic activity as compared with other materials [99]. Moreover, it was revealed that the properties of graphene can be tailored to satisfy the improved requirements of fuel cells. Although the researches on the catalytic activities of N-doped carbonaceous materials started in 1926, intensive study appears recently for N-doped graphene aim to achieving a perfect electrocatalyst with excellent performance [100,101].

The ORR process in fuel cells has been intensively discussed in many articles that reported in the past few years. The electrocatalytic mechanism of N-doped graphene was firstly studied by using density functional theory [102], and two pathways were proposed in ORR process. Zhang et al. reported that oxygen reduction followed a four electron pathway [103], which reduced to water in acidic environment, and the N doping introduces asymmetry spin density and atomic charge density, making it possible for N-doped graphene to show high electrocatalytic activities for ORR process. Lin et al. also pointed that N-doped graphene has high electrocatalytic activity toward ORR in alkaline electrolyte via a favorable four electron pathway for the formation of water [39], leading to high performance and low polarization loss. Oxygen reduced into OH^- in alkaline medium was also reported by Liu et al. [35], and the achieved activities are equivalent to those of state-of-the-art Pt/C. At the same time, a two electron pathway in which oxygen is partly reduced into H_2O_2 in acidic environment was reported by Kurak and his co-workers [102], which represents for the dissociative and associative mechanisms [104].

The theoretical simulations of N-doped graphene for ORR processes were well confirmed by the experimental studies, and N-doped graphene was proved to be an efficient metal-free electrocatalyst in fuel cells [11,105]. This may be because of that (1) a large number of structural defects can be produced through the N doping of graphene, and these defects can act as the electroactive sites for catalyzing the ORR process [106]; (2) the N doping can enhance the electrical conductivity of N-doped graphene, ensuring the fast electron transfer [107]; (3) the unique structure of N-doped graphene can allow the smooth penetration of electrolyte and enhance the contact area between electrocatalysts and electrolyte. Toward this regard, Qu et al. recently demonstrated that the steady-state catalytic current at the N-doped graphene electrode was found to be about 3 times higher than that of Pt/C electrode over a large potential range [11], as clearly illustrated in Fig. 10. Also, Lin et al. showed that N-doped graphene displays

excellent long-term stability and resistance to methanol oxidation, offering performance superior to those of a commercial Pt/C electrocatalyst [39]. Moreover, previous reports displayed that the N-doped graphene exhibits an n-type behavior, indicating that substitutional N doping can effectively modulate the electrical properties of graphene, so the high carrier mobility, high doping level, and reliable N-doped behavior in both air and vacuum were obtained [12,15]. Based on this, Yang et al. developed a facile and a powerful approach to fabricate N-doped graphene sheets with high specific area [40], which would responsible for the excellent electrocatalytic activity toward the ORR process. Additionally, N atoms and other heteroatoms co-doped graphene was also prepared, and the resultant materials can also serve as the efficient metal-free electrocatalysts for ORR [26,32].

Besides the direct utilization of N-doped graphene in fuel cells, N-doped graphene was also investigated as carbon support material for electrocatalysts. The N-doped graphene can enhance the electrical conductivity of hybrid electrocatalysts, prevent the aggregation and improve the structural integrity of electroactive catalysts. The synergistic effects of all the above functions contribute to the significantly improved electrocatalytic activity of the hybrid electrocatalysts. For instances, Pt is the ideal electrocatalyst for catalyzing the electrocatalytic activity in fuel cells, and it was confirmed that little amount of Pt nanoparticles supported on N-doped graphene could further enhance the electrocatalytic activity obviously. Xiong et al. synthesized Pt/N-doped graphene via a heat treatment method [22], and the electrocatalyst demonstrates superior catalytic activity for methanol electrical oxidation process, with a peak current density of 0.218 A mg_{pt}^{-1}, which is about five times higher than an un-doped Pt/graphene control electrocatalyst [24]. Xin et al. prepared Pt/N-doped graphene by the microwave method, and the electrocatalysts exhibited much higher electrochemical active surface area [63], methanol catalytic activity, and tolerance to CO poisoning than those of the Pt/graphene under fuel cell conditions. Other inorganic materials hybridized with N-doped graphene were also synthesized, and they displayed excellent performances in fuel cells. For instances, FeCo [37] and Fe_3O_4 [54] deposited on N-doped graphene were synthesized through heat treatment and hydrothermal method, respectively, and both exhibited efficient electrocatalytic activities for the oxygen reduction processes in fuel cells.

Additionally, the electrocatalytic activities of N-doped graphene hybridized with other carbonaceous materials were investigated. Liu et al. prepared N-doped graphene/carbon composite as non-precious metal electrocatalyst, and revealed that the hybrid composite can efficiently catalyze the oxygen reduction process [35].

4.2. Secondary batteries

Lithium-ion batteries (LIBs) are the most widely investigated secondary batteries, and are expected to provide high performance for the smart electronics, electric vehicles and hybrid electric vehicles. The discovery of carbonaceous materials, such as carbon nanotubes (CNTs), supplies a chance for the development of LIBs [108–110]. Moreover, the appearance of graphene made LIBs a hot topic in the past several years [111]. Recently, N-doped graphene was synthesized and utilized as the anode materials for LIBs. Since a large number of the structural defects were induced during the process of N doping, the reversible discharge capacity of N-doped graphene (approximate 1043 mAh g^{-1} at a low charge/discharge rate of 50 mA g^{-1}) is almost twice higher than that of pristine graphene [28]. Even compared with the B-doped graphene, N-doped graphene also shows the comparable electrochemical performance, in terms of discharge capacity and rate capability [28], as presented in Fig. 11. It was confirmed that the number of Li^+ plays a key role on the discharge capacity. The greatly-increased active sites induced by N doping can provide much more interaction sites, thus facilitating the anchoring of Li^+. Furthermore, Cho et al. reported that both pyridinic N and pyrrolic N structures can be effective for Li^+ intercalation [14], and experimental results show that the large storage capacity of both N-doping structures comes from the formation of dangling bonds that originated from the rearrangement of the C and N atoms [20]. High power and energy densities can be simultaneously obtained by using N-doped graphene anodes. The special properties allow rapid surface Li^+ absorption and ultrafast Li^+ diffusion and electron transfer, making this material superior to conventional anode materials based on Li^+ intercalation reactions [28,111].

Similar to N-doped graphene, the N and B co-doped graphene is expected to have further enhanced properties [20]. Early studies have shown that B-substituted disordered carbons can store more Li^+ than pristine carbons, owning to the abundant active sites induced by boron atoms [112]. So when graphene was doped with both N and B atoms, they could display further enhanced lithium storage performance. This was already experimentally confirmed by Panchakarla and his co-workers [113].

Recently, N-doped graphene materials with various structures were also investigated as the anode materials for LIBs. For instances, Lu and his co-workers synthesized the N-doped graphene frameworks with active functional groups as the cathode materials of LIBs [114]. Electrochemical measurements revealed that the cathode can deliver a high reversible capacity of 146 mAh g^{-1} at 50 mA g^{-1} after 1000 cycles. Moreover, Feng et al. prepared the bipolar N-doped graphene frameworks as the cathode for LIBs [115], and the cathode exhibits an extremely high specific capacity of 379 mAh g^{-1} at 0.5 A g^{-1} for 2500 cycles. This performance is superior to most of the reported LIBs cathode materials. Mesoporous N-doped graphene aerogels were also reported by Zheng and his co-workers [116]. Benefiting from the hierarchical porous structures, abundant active sites and high electrical conductivity, the resultant LIBs exhibit greatly enhanced rate capability and cycling stability.

N-doped graphene can also hybridize with other materials as the electrodes of LIBs. By date, various inorganic materials decorated N-doped graphene composites were synthesized through different methods. For instances, MnO/N-doped graphene sheets [25], VO_2/N-doped graphene [53], Zn_2GeO_4/N-doped graphene [61], CuO/N-doped graphene [82], SnO_2/N-doped graphene [95,117], NiO/N-doped graphene [118], Fe_3O_4/N-doped graphene [119], TiO_2/N-doped graphene [120], and Si/N-doped graphene [121] structures were prepared as the anode materials. The N-doped graphene has several advantages for the construction of hybrid materials. Firstly, the presence of N-doped graphene nanosheets can prevent the severe aggregation of nanoparticles, and provide much more contact areas between the nanoparticles and electrolyte. Secondly, N-doped graphene can enhance the electrical conductivity of hybrid materials and boost the electron transfer during charge/discharge processes. Thirdly, N-doped graphene can contribute certain discharge capacities in the total capacity of electrode materials. Last by not least, the N-doped graphene can bind well with inorganic nanoparticles, and thus well maintaining the integrity and stability of electrode materials during electrochemical tests. Thus, when N-doped graphene based hybrid materials were used as the electrode materials for LIBs, they could exhibit significantly enhanced electrochemical performances as compared with those of the bare counterparts.

Sodium ion batteries (SIBs) have attracted tremendous attention due to natural abundance and low cost of sodium sources [122]. N-doped graphene material was also used in the SIBs. Unfortunately, the larger radius (0.97 Å) of Na ion, 55% larger than that of Li^+ [123], makes rapid Na^+ intercalation/extraction in N-doped graphene materials difficult [124]. Besides the kinetic issue,

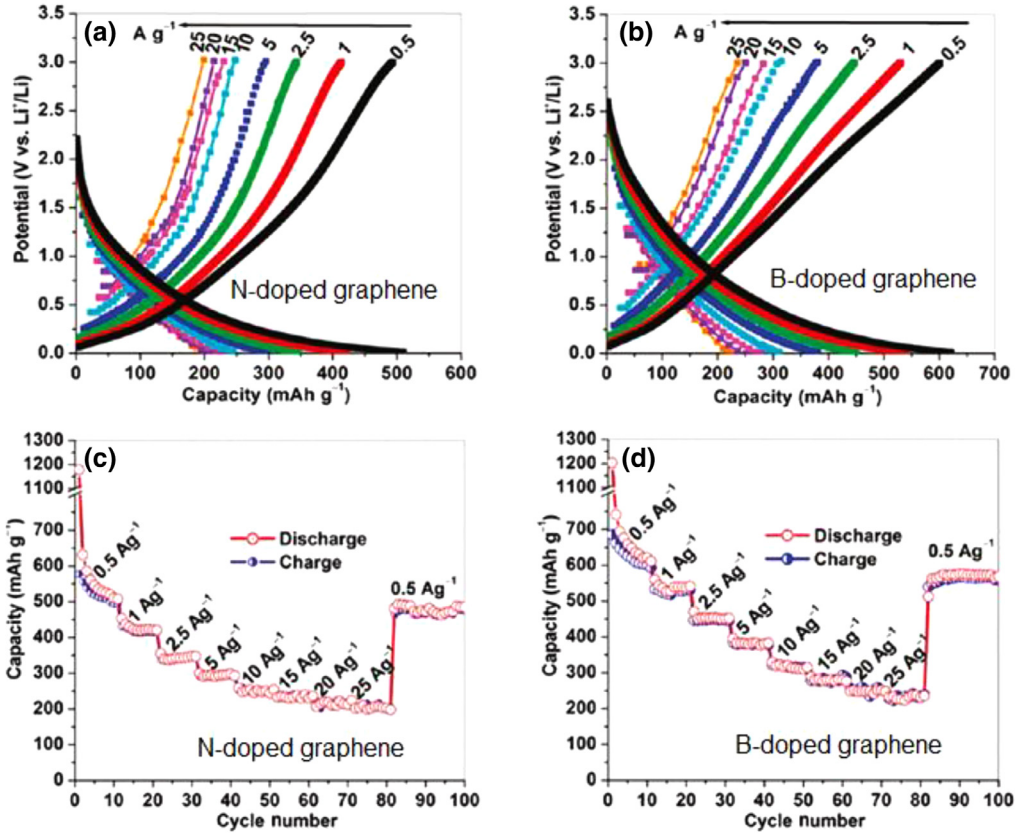

Fig. 11. Lithium storage performance comparisons of N-doped and B-doped graphene. (a) and (b) Galvanostatic charge-discharge profiles of (a) N-doped and (b) B-doped graphene electrodes. (c) and (d) Rate capabilities and cycle performance of (c) N-doped and (d) B-doped graphene electrodes obtained over a wide range of high current densities, from 0.5 to 25 A g^{-1}. The charge–discharge profiles in (a) and (b) correspond to the 10th cycle charge–discharge profiles at each current density between 0.5 and 25 A g^{-1} in (c) and (d), respectively [28].

the larger Na^+ radius is also relevant for structural change during insertion or extraction. Nevertheless, remarkable progress was also achieved for N-doped graphene materials.

Ju and his co-workers investigated the electrochemical performance of Na^+ intercalation/extraction in N-doped graphene nanosheets [125]. Due to the large structure defects induced by N doping, the resultant N-doped graphene nanosheets exhibit superior Na^+ storage capacity of 260 mAh g^{-1} at 50 mA g^{-1}, good rate capability and excellent cycle performance even at 500 mA g^{-1}. Recently, 3D N-doped graphene structures were also utilized as the anode materials for SIBs. For instances, N-doped graphene/carbon hybrid was adopted as the anode material for SIBs with excellent rate performance [126]. Dai et al. fabricated a 3D N-doped graphene foam as the anode materials for SIBs [127]. As shown in Fig. 12, the resultant anode material delivered an unusually high initial reversible capacity of 852.6 mAh g^{-1} at 500 mA g^{-1}, accompanying with a long-life cycle stability. Moreover, 3D free-standing N-doped graphene aerogel was also prepared for the high-performance anode materials of SIBs [128]. The observed superb performance of the N-doped graphene anode in SIBs was attributed to synergistic effects associated with the 3D mesoporous structure with a well-defined porosity, large surface area, and enlarged lattice spacing between graphene layers, coupled with the N doping induced defects, to facilitate the diffusion of the large-size sodium ions, enhance the storage of sodium ions, and minimize the effect of volume expansion during discharge–charge processes.

Similarly, N-doped graphene/inorganic material hybrids were also reported as the anode materials for SIBs. In a typical sample, amorphous phosphorus/N-doped graphene paper was synthesized and utilized as the anode material for SIBs [129]. The resultant anode exhibits an ultra-stable cyclic performance and excellent rate capability in SIBs. It was revealed that the N-doped graphene not only contributes to an increase in capacity for sodium storage, but also is beneficial in regards to improved rate performance of the anode. Moreover, other inorganic materials, including $Na_3V_2(PO_4)_3$ [130], SnO_2 nanoparticles [131], and CNTs@SnO_2 composite [132], were also reported to hybridize with N-doped graphene nanosheets, and the electrochemical measurements demonstrated that all the hybrid materials show the greatly enhanced electrochemical performance in sodium storage.

4.3. Supercapacitor

Supercapacitor is an alternative energy storage system, and it has attracted increasing attention in recent years due to their intrinsic features of high power and energy density, ultra-long cycle life and low maintenance cost [133]. Supercapacitors store and release electrical energy based on the electrostatic interactions between ions in the electrolyte and electrodes, while LIBs depends on the chemical conversion reactions in the charge/discharge process [20,47]. Based on their different charge-storage mechanisms, supercapacitors can be divided into pseudo-capacitors and electrical double-layer capacitors [134]. However, the poor cycling stability, electrical conductivity and high cost would limit the further application of pseudo-capacitors because of the unideal performance of redox-active materials, which are essential materials for pseudo-capacitors. On the contrary, the appearance of carbon materials supplied a chance for developing double-layer capacitors.

Carbon nanotubes used for supercapacitors was firstly reported in the past several years. As graphene been discovered, reports

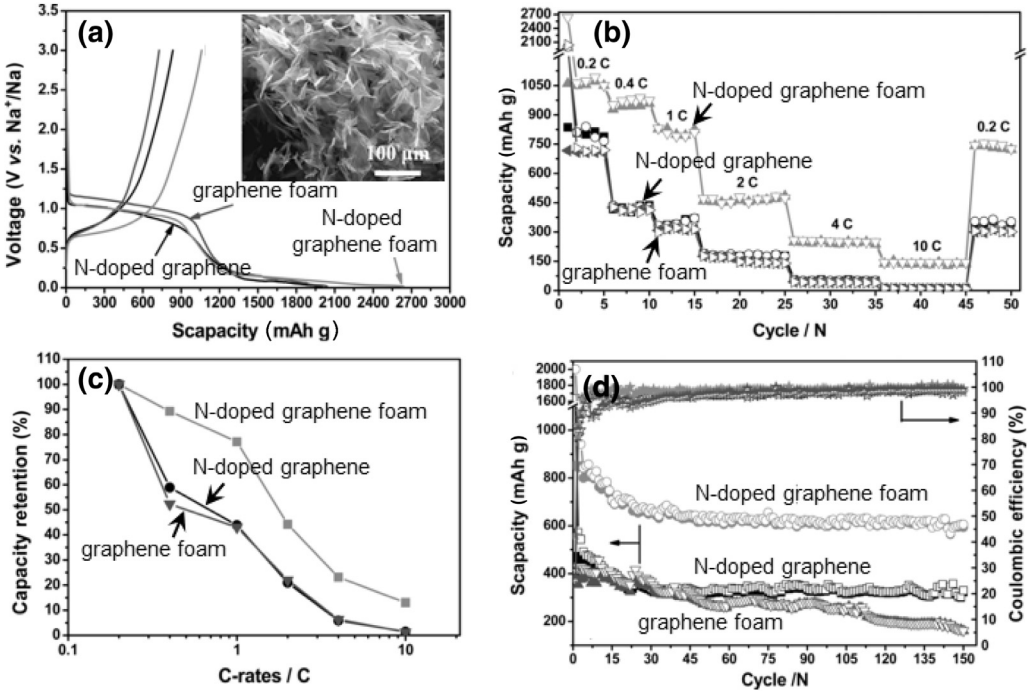

Fig. 12. Sodium storage performance of N-doped graphene foam. (a) Initial charge-discharge curves of the N-doped graphene foam, graphene foam, and N-doped graphene at 0.2 C. The inset of (a) shows the typical morphology of N-doped graphene foam. (b) Rate performance of the N-doped graphene foam, graphene foam, and N-doped graphene from 0.2 C to 10 C. (c) Capacity retention of the initial capacity at 0.2 C vs. C-rate and (d) cycling performance of the N-doped graphene foam, graphene foam, and N-doped graphene at 1.0 C within the voltage range of 0.02–3.0 V (assumed 1.0 C = 500 mA g^{-1}) [127].

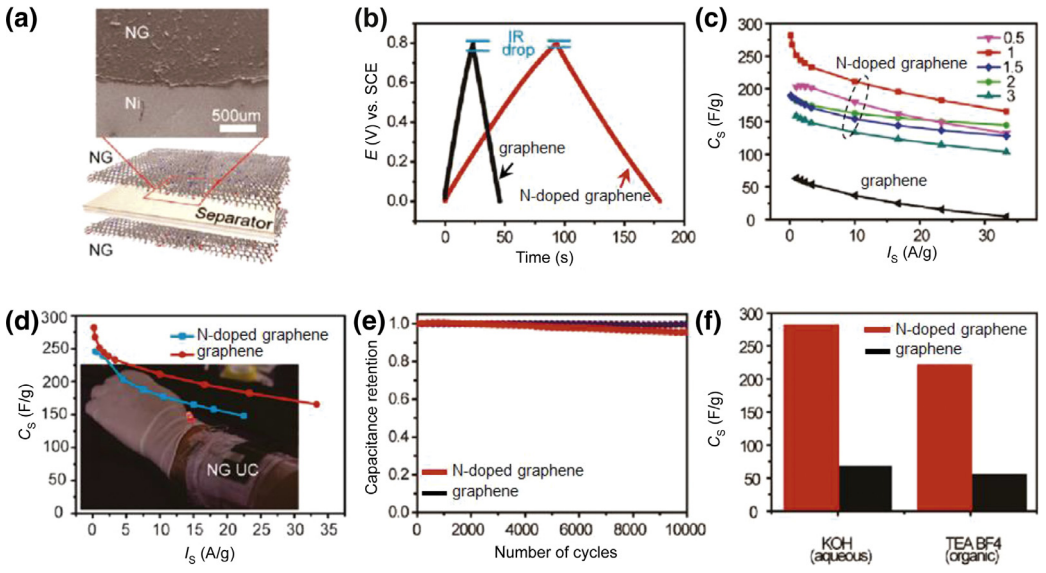

Fig. 13. Supercapacitors based on N-doped graphene and their electrochemical testing. (a) A schematic illustration of the assembled supercapacitor structure alongside a SEM image showing a top view of the device. (b) Charge–discharge curves measured by galvanostatic characterization. (c) Gravimetric capacitances of supercapacitors based on various N-doped graphene and pristine graphene measured at a series of current densities. (d) Gravimetric capacitances of supercapacitors built on nickel and paper substrates measured at a series of current densities. The inset of (d) shows a wearable supercapacitor wrapped around a human arm can store the electrical energy to light up a light emitting diode. (e) The cycling tests for the supercapacitors based on Ni and paper substrates up to 10,000 cycles. (f) The specific capacitances measured in aqueous and organic electrolytes. The mass loading of N-doped graphene is 1.0 mg cm^{-2} [47].

on this novel material for supercapacitors appeared [135,136]. N-doped graphene usually possesses large surface area, and it has been suggested that the N functionalization could change the donor/acceptor characteristics of graphene [47,64]. Moreover, the N doping can produce large amounts of structural defects, and these defects can serve as active sites for storing electrons. Both of these merits contributed to the enhanced capacitive performance of N-doped graphene. Fig. 13 shows the supercapacitor based on N-doped graphene and the electrochemical testing results. At the same time, Jeong et al. prepared N-doped graphene for high-performance supercapacitors and investigated the importance of N-doped sites at basal planes [47]. In this article, they prepared the N-doped graphene via a simple plasma process, and the achieved capacitance are about 4 times larger than those of pristine graphene without sacrificing other essential and useful properties for supercapacitors. Qiu et al. investigated the highly

conductivity of N-doped graphene sheets [29], and showed that all the synthesis methods can produce N-doped graphene, but not all the achieved N-doped graphene can be suitable for supercapacitors. Among those methods, the graphene sheets prepared from flame treatment method possess more defects due to the environmental conditions and introduction of N atoms, which makes it a promising candidate for supercapacitors [64]. N doping via hydrothermal method and microwave-assisted hydrothermal method were also used as the materials of supercapacitors, and N-doped graphene exhibited excellent supercapacitive properties [52,59,137].

N-doped graphene supplied as support materials were investigated in few articles. For instances, Liu et al. adopted microwave-assisted hydrothermal method to prepare N-doped graphene/Mn_3O_4 material [60], and showed promising enhancement in both energy and power densities. Fe_3O_4 decorated on N-doped graphene was prepared, and the resultant material displays excellent performance when been utilized as the electrode materials for supercapacitors [54]. Moreover, 3D N-doped graphene/CNT networks for supercapacitors were synthesized, and the materials show high specific capacitance, good rate capability and good durability [138]. Therefore, it can be concluded that the materials based on N-doped graphene are promising candidates for supercapacitors.

4.4. Other applications

Nowadays, besides the above mentioned applications, N-doped graphene have been also used in other promising fields, including field-effect transistors (FET) [19,43,65,139], quencher of the materials for photoluminescence [21,27], high-performance polymer light-emitting diodes [48], rewritable nonvolatile memory materials [49], medical applications [50,93], electrochemical bio-sensing [45], vanadium redox flow batteries [140], and catalysts supporters of photocatalysis [27]. For instances, Fan et al. developed an electrochemical bisphenol A sensor based on N-doped graphene nanosheets for the detection of bisphenol A [50]. N-doped grahene/CdS heterostructures as photocatalyst for splitting water under visible light irradiation was also prepared, and it exhibits great catalytic activity [30]. Additionally, since N-doped graphene possesses many intriguing properties, it is expected that new applications related energy fields can be exploited and developed in the near future.

5. Conclusions, challenges and perspective

This review summarized the synthesis methods and characterization techniques for N-doped graphene. For the applications of N-doped graphene, different methods could generate different properties, and the methods play a key role on the special properties that suitable for certain applications. N-doped graphene hybridized with inorganic composites can exhibit enhanced properties and improved performances due to the synergetic effects between N-doped graphene and inorganic nanoparticles, thus can be widely used in the fields of energy, analytical, medicine, biotechnology, and pollutants removal applications. Especially, the energy applications are of significance, such as the electrocatalysts in fuel cells and electrode materials for LIBs, SIBs and supercapacitors. It is expected that N-doped graphene can be used as the promising candidate for the clean and renewable energy sources in the future.

However, in spite of the great research progress in N-doped graphene, there are still many issues to be solved, such as:

(1) For the synthesis of N-doped graphene, how to controllably synthesize specific type N-doped graphene with high content (>90%) of pyridine N (or other types of N species) for specific applications? Moreover, novel synthesis methods under mild and environment-friendly conditions should be exploited, so the N-doped graphene can be produced in large scale.

(2) For the detailed characterization of N-doped graphene, how to accurately identify the specific type of N species and how to build precise theoretical calculation models to understand the functions of specific N species? Moreover, how to *in-situ* characterize the formation mechanisms of N sites during the synthesis processes?

(3) For the applications of N-doped graphene, which type of N doping plays the crucial role in the performance enhancements? The relationship between the types of N doping and the properties of N-doped graphene needs to be clarified, so that more desirable properties for special applications could be achieved. Additionally, the detailed mechanisms of the applications for N-doped graphene should be systematically investigated, thus the applications would be practical and widespread.

Since there are many problems to be solved, more attention and further research efforts are required from physics, chemistry and material science fields.

Acknowledgments

This work is supported by the National Key R&D Program of China (2017YFA0208200, 2016YFB0700600, 2015CB659300), Projects of NSFC (21403105, 21573108), Anhui Provincial Key Research and Development Program (1704A0902022), Natural Science Foundation of Jiangsu Province (BK20150583, BK20160647) and the Fundamental Research Funds for the Central Universities (020514380107).

References

[1] A.K. Geim, K.S. Novoselov, Nat. Mater. 6 (2007) 183–191.
[2] C. Lee, X.D. Wei, J.W. Kysar, J. Hone, Science 321 (2008) 385–388.
[3] A.K. Geim, Science 324 (2009) 1530–1534.
[4] K.S. Novoselov, A.K. Geim, S.V. Morozov, D. Jiang, Y. Zhang, S.V. Dubonos, I.V. Grigorieva, A.A. Firsov, Science 306 (2004) 666–669.
[5] Y.J. Hu, P. Wu, C.X. Cai, Electrochim. Acta 85 (2012) 314–321.
[6] S.J. Guo, D. Wen, Y.M. Zhai, S.J. Dong, E.K. Wang, ACS Nano 4 (2010) 3959–3968.
[7] P.C. Lian, X.F. Zhu, H.F. Xiang, Z. Li, E.S. Yang, H.H. Wang, Electrochim. Acta 56 (2010) 834–840.
[8] L.L. Li, K.P. Liu, G.H. Yang, C.M. Wang, J.R. Zhang, J.J. Zhu, Adv. Funct. Mater. 21 (2011) 869–878.
[9] Z.B. Wang, C.R. Zhao, P.F. Shi, Y.S. Yang, Z.B. Yu, W.K. Wang, G.P. Yin, J. Phys. Chem. C 1 (2010) 114–119.
[10] K.P. Gong, F. Du, Z.H. Xia, M. Durstock, L.M. Dai, Science 323 (2009) 760–764.
[11] L.T. Qu, Y. Liu, J.B. Baek, L.M. Dai, ACS Nano 3 (2010) 1321–1326.
[12] D.H. Wei, Y.Q. Liu, Y. Wang, H.L. Zhang, L.P. Huang, G. Yu, Nano Lett. 5 (2009) 1752–1758.
[13] Y.J. Cho, H.S. Kim, S.Y. Baik, Y. Myung, C.S. Jung, C.H. Kim, J.H. Park, H.S. Kang, J. Phys. Chem. C 115 (2011) 3737–3744.
[14] Y.J. Cho, H.S. Kim, H. Im, Y. Myung, G.B. Jung, C.W. Lee, J. Park, M.H. Park, J. Cho, H.S. Kang, J. Phys. Chem. C 115 (2011) 9451–9457.
[15] Y.Z. Xue, B. Wu, L. Jiang, Y.L. Guo, L.P. Huang, J.Y. Chen, J.H. Tan, D.H. Geng, B.R. Luo, W.P. Hu, G. Yu, Y.Q. Liu, J. Am. Chem. Soc. 134 (2012) 11060–11063.
[16] Z. Jin, J. Yao, C. Kittrell, J.M. Tour, ACS Nano 5 (2011) 4112–4117.
[17] R.T. Lv, Q. Li, A.R. Botello-Mendez, T. Hayashi, B. Wang, A. Berkdemir, Q.Z. Hao, A.L. Elias, R. Cruz-Silva, H.R. Gutuerrez, Y.A. Kim, H. Muramatsu, J. Zhu, M. Endo, H. Terrones, J.C. Charlier, M.H. Pan, M. Terrones, Sci. Rep. 2 (2012) 586.
[18] H. Gao, L. Song, W.H. Guo, L. Huang, D.Z. Yang, F.C. Wang, Y.L. Zuo, X.L. Fan, Z. Liu, W. Gao, R. Vajtai, K. Hackenberg, P.M. Ajayan, Carbon 50 (2012) 4476–4482.
[19] O.S. Kwon, S.J. Park, J.Y. Hong, A.R. Han, J.S. Lee, J.H. Oh, J. Jang, ACS Nano 6 (2012) 1486–1493.
[20] A.M. Reddy, A. Srivastava, S.R. Gowda, H. Gullapalli, M. Dubey, P.M. Ajayan, ACS Nano 4 (2012) 6337–6342.
[21] M. Li, Z.S. Wu, W.C. Ren, H.M. Cheng, N.J. Tang, W.B. Wu, W. Zhong, Y.W. Du, Carbon 50 (2012) 5286–5291.

[22] B. Xiong, Y.K. Zhou, Y.Y. Zhao, J. Wang, X. Chen, R. O'Hayre, Z.P. Shao, Carbon 52 (2013) 181–192.
[23] X.L. Li, H.L. Wang, J.T. Robinson, H. Sanchez, G. Diankov, H.J. Dai, J. Am. Chem. Soc. 131 (2009) 15939–15944.
[24] B. Xiong, Y.K. Zhou, R. Hayre, Z.P. Shao, Appl. Surf. Sci. 266 (2013) 433–439.
[25] K.J. Zhang, P.G. Han, L. Gu, L.X. Zhang, Z.H. Liu, Q.S. Kong, C.J. Zhang, S.M. Dong, Z.Y. Zhang, J.H. Yao, H.X. Xu, G.L. Cui, L.Q. Chen, ACS Appl. Mater. Interfaces 4 (2012) 658–664.
[26] S.B. Yang, L.J. Zhi, K. Tang, X.L. Feng, J. Maier, K. Mullen, Adv. Funct. Mater. 22 (2012) 3634–3640.
[27] T.V. Khai, H.G. Na, D.S. Kwak, H. Ham, K.B. Shim, H.W. Kim, Carbon 50 (2012) 3799–3806.
[28] Z.S. Wu, W.C. Ren, L. Xu, F. Li, H.M. Cheng, ACS Nano 5 (2011) 5463–5471.
[29] Y.C. Qiu, X.F. Zhang, S.H. Yang, Phys. Chem. Chem. Phys. 13 (2011) 12554–12558.
[30] L. Jia, D.H. Wang, Y.X. Huang, A.W. Xu, H.Q. Yu, J. Phys. Chem. C 115 (2011) 11466–11473.
[31] B.D. Guo, Q. Liu, E.D. Chen, H.W. Zhu, L. Fang, J.R. Gong, Nano Lett. 10 (2010) 4975–4980.
[32] S.Y. Wang, L.P. Zhang, Z.H. Xia, A. Roy, D.W. Chang, J.B. Baek, L.M. Dai Angew, Chem. Int. Ed. 51 (2012) 4209–4212.
[33] J. Zhong, J.J. Deng, B.H. Mao, T. Xie, X.H. Sun, Z.G. Mou, C.H. Hong, P. Yang, S.D. Wang, Carbon 50 (2012) 321–341.
[34] Z.L. Li, J.H. Liu, Z.W. Huang, Y. Yang, C.G. Xia, F.W. Li, ACS Catal. 3 (2013) 839–845.
[35] D.S. Geng, S.L. Yang, Y. Zhang, J.L. Yang, J. Liu, R.Y. Li, T.K. Sham, X.L. Sun, S.Y. Ye, S. Knight, Appl. Surf. Sci. 257 (2011) 9193–9198.
[36] Q. Li, H.Y. Zhang, H.W. Zhong, S.M. Zhang, S. Chen, Electrochim. Acta 81 (2012) 313–320.
[37] X.G. Fu, Y.R. Liu, X.P. Cao, J.T. Jin, Q. Liu, J.Y. Zhang, Appl. Catal. B Environ. 130 (2013) 143–151.
[38] H.L. Peng, Z.Y. Mo, S.J. Liao, H.G. Liang, L.J. Yang, F. Luo, H.Y. Song, Y.L. Zhong, B.Q. Zhang, Sci. Rep. 3 (2013) 1765–1771.
[39] Z.Y. Lin, G.H. Waller, Y. Liu, M.L. Liu, C.P. Wong, Nano Energy 2 (2013) 241–248.
[40] S.Y. Yang, K.H. Chang, Y.L. Huang, Y.F. Lee, H.W. Tien, S.M. Li, Y.H. Lee, C.H. Liu, C.C.M. Ma, C.C. Hu, Electrochem. Commun. 14 (2012) 39–42.
[41] Z.Y. Lin, M.K. Song, Y. Ding, Y. Liu, M.L. Liu, C.P. Wong, Phys. Chem. Chem. Phys. 14 (2012) 3381–3387.
[42] L. Guan, L. Cui, K. Lin, Y.Y. Wang, X.T. Wang, F.M. Jin, F. He, X.P. Chen, S. Cui, Appl. Phys. A 102 (2011) 289–294.
[43] D.J. Late, A. Ghosh, K.S. Subrahmanyam, L.S. Panchakarla, S.B. Krupanidhi, C.N.R. Rao, Solid State Commun. 150 (2010) 734–738.
[44] N. Li, Z.Y. Wang, K.K. Zhao, Z.J. Shi, Z.N. Gu, S.K. Xu, Carbon 48 (2010) 255–259.
[45] Y. Wang, Y.Y. Shao, D.W. Matson, J.H. Li, Y.H. Lin, ACS Nano 4 (2010) 1790–1798.
[46] N. Soin, S.S. Roy, S. Roy, K.S. Hazra, D.S. Misra, T.H. Lim, C.J. Hetherington, J.A. Malaughlin, J. Phys. Chem. C 115 (2011) 5366–5372.
[47] H.M. Jeong, J.W. Lee, W.H. Shin, Y.J. Choi, H.J. Shin, J.K. Kang, J.W. Choi, Nano Lett. 11 (2011) 2472–2477.
[48] J.O. Hwang, J.S. Park, D.S. Choi, J.Y. Kim, S.H. Lee, K.E. Lee, Y.H. Kim, M.H. Song, S. Yoo, S.O. Kim, ACS Nano 6 (2012) 159–167.
[49] S. Seo, Y.H. Yoon, J.H. Lee, Y.H. Park, H. Lee, ACS Nano 7 (2013) 3607–3615.
[50] H.X. Fan, Y. Li, D. Wu, H.M. Ma, K.X. Mao, D.W. Fan, B. Du, H. Li, Q. Wei, Anal. Chim. Acta 711 (2012) 24–28.
[51] B.J. Jiang, C.G. Tian, L. Wang, L. Sun, C. Chen, X.Z. Nong, Y.J. Qiao, H.G. Fu, Appl. Surf. Sci. 258 (2012) 3438–3443.
[52] L. Sun, L. Wang, C.G. Tian, T.X. Tan, Y. Xie, K.Y. Shi, M.T. Li, H.G. Fu, RSC Adv. 2 (2012) 4498–4506.
[53] C. Nethravathi, C.R. Rajamathi, M. Rajamathi, U.K. Gautam, X. Wang, D. Golberg, Y. Bando, ACS Appl. Mater. Interfaces 5 (2013) 2708–2714.
[54] Z.S. Wu, S.B. Yang, Y. Sun, K. Parvez, X.L. Feng, K. Mullen, J. Am. Chem. Soc. 134 (2012) 9082–9085.
[55] J.C. Bai, Q.Q. Zhu, Z.X. Lv, H.Z. Dong, J.H. Yu, L.F. Dong, Int. J. Hydrogen Energy 38 (2013) 1413–1418.
[56] D.H. Deng, X.L. Pan, L. Yu, Y. Cui, Y.P. Jiang, J. Qi, W.X. Li, Q. Fu, X.C. Ma, Q.K. Xue, G.G. Sun, X.H. Bao, Chem. Mater. 23 (2011) 1188–1193.
[57] C.H. Choi, S.H. Park, M.W. Chung, S.I. Woo, Carbon 55 (2013) 98–107.
[58] Z. Jin, Z.Z. Sun, L.J. Simpson, K.J. O'Neal, P.A. Parilla, Y. Li, N.P. Stadie, C.C. Ahn, C. Kittrell, J.M. Tour, J. Am. Chem. Soc. 132 (2010) 15246–15251.
[59] Y.H. Lee, K.H. Chang, C.C. Hu, J. Power Sources 227 (2013) 300–308.
[60] C.L. Liu, K.H. Chang, C.C. Hu, W.C. Wen, J. Power Sources 217 (2012) 184–192.
[61] F. Zou, X.L. Hu, Y.M. Sun, W. Luo, F.F. Xia, L. Qie, Y. Jiang, Y.H. Huang, Chem. Eur. J. 19 (2013) 6027–6033.
[62] Y.J. Zhang, K. Fugane, T. Mori, L. Niu, J.H. Ye, J. Mater. Chem. 22 (2012) 6575–6580.
[63] Y.C. Xin, J.G. Liu, X. Jie, W.M. Liu, F.Q. Liu, Y. Yin, J. Gu, Z.G. Zou, Electrochim. Acta 60 (2012) 354–358.
[64] Y.P. Zhang, B. Cao, B. Zhang, X. Qi, C.X. Pan, Thin Solid Films 520 (2012) 6850–6855.
[65] W. Qian, X. Cui, R. Hao, Y.L. Hou, Z.Y. Zhang, ACS Appl. Mater. Interfaces 3 (2011) 2259–2264.
[66] D.P. He, Y.L. Jiang, H.F. Lv, M. Pan, S.C. Mu, Appl. Catal. B Environ 132 (2013) 379–388.
[67] X.L. Wang, Z.F. Hou, T. Lkeda, M. Oshima, M.A. Kakimoto, K. Terakura, J. Phys. Chem. A 117 (2013) 579–589.
[68] Z.Q. Luo, S. Lim, Z.Q. Tian, J.Z. Shang, L.F. Lai, B. MacDonald, C. Fu, Z.X. Shen, T. Yu, J.Y. Lin, J. Mater. Chem. 21 (2011) 8038–8044.
[69] L.S. Zhang, X.Q. Liang, W.G. Song, Z.Y. Wu, Phys. Chem. Chem. Phys. 12 (2010) 12055–12059.
[70] B. Huang, Phys. Lett. A 375 (2011) 845–848.
[71] D.S. Geng, Y. Chen, Y.G. Chen, Y.L. Li, R.Y. Li, X.L. Sun, S.Y. Ye, S.N. Knight, Energy Environ. Sci. 4 (2011) 760–764.
[72] H.B. Wang, C.J. Zhang, Z.H. Liu, L. Wang, P.X. Han, H.X. Xu, K.J. Zhang, S.M. Dong, J.H. Yao, G.L. Cui, J. Mater. Chem. 21 (2011) 5430–5434.
[73] X.S. Zhou, L.J. Wan, Y.G. Guo, Adv. Mater. 25 (2013) 2152–2157.
[74] D.H. Wu, Y.F. Li, Z. Zhou, Theor. Chem. Acc. 130 (2011) 209–213.
[75] Z.H. Wen, X.C. Wang, S. Mao, Z. Bo, H. Kim, S.M. Cui, G.H. Lu, X.L. Feng, J.H. Chen, Adv. Mater. 24 (2012) 5610–5616.
[76] P. Chen, J.J. Yang, S.S. Li, Z. Wang, T.Y. Xiao, Y.H. Qian, S.H. Yu, Nano Energy 2 (2013) 249–256.
[77] L.N. Zhang, L. Li, C. Ma, S.G. Ge, M. Yan, C. Bian, Sens. Actuat. B 221 (2015) 799–806.
[78] Y.Q. Sun, Q. Wu, G.Q. Shi, Energy Environ. Sci. 4 (2011) 1113–1132.
[79] P.L. Subrahmanyam, L.S. Panchakarla, A. Govindaraj, C.N.R. Rao, J. Phys. Chem. C 113 (2009) 4257–4259.
[80] S. Bai, X.P. Shen, G.X. Zhu, M.Z. Li, H.T. Xi, K.M. Chen, ACS Appl. Mater. Interfaces 4 (2012) 2378–2386.
[81] Z.Y. Liu, G.X. Zhang, Z.Y. Lu, X.Y. Jin, Z. Chang, X.M. Sun, Nano Res. 6 (2013) 293–301.
[82] J.X. Chen, D.L. Zhao, R.R. Yao, C. Li, X.J. Wang, F.F. Sun, J. Alloy Compds. 714 (2017) 419–424.
[83] B. Zhang, P. Hermet, L. Henrard, ACS Nano 4 (2010) 4165–4173.
[84] S.O. Guillaume, B. Zheng, J.C. Charlier, L. Henratd, Phys. Rev. B 85 (2012) 035444.
[85] Y. Qin, J. Yuan, J. Li, D.C. Chen, Y. Kong, F.Q. Chu, Y.X. Tao, M.L. Liu, Adv. Mater. 27 (2015) 5171–5175.
[86] F. Parvizi, D. Tewelddebrhan, S. Dhosh, I. Calizo, A.A. Balandin, H. Zhu, R. Abbaschian, Micro Nano Lett. 3 (2008) 29–34.
[87] D.X. Yang, A. Velamakanni, G. Bozoklu, S.J. Park, M. Stoller, R.D. Piner, S. Stankovich, I. Jung, D.A. Field, C.A. Ventrice, R.S. Ruoff, Carbon 47 (2009) 145–152.
[88] D.H. Lee, W.J. Lee, S.O. Kim, Y.H. Kim, Phys. Rev. Lett. 106 (2011) 175502.
[89] H. Hibini, H. Kageshima, M. Kotsugi, F. Maeda, F.Z. Guo, Y. Watanabe, Phys. Rev. B 79 (2009) 125437–125441.
[90] D. Usachov, O. Vilkov, A. Gruneis, D. Haberer, A. Fedorov, V.K. Adamchuk, A.B. Preobrajenski, P. Dudin, A. Barinov, M. Oehzelt, C. Laubschat, D.V. Vyalikh, Nano Lett. 11 (2011) 5401–5407.
[91] N. Hellgren, J. Guo, C. Sathe, A. Agui, J. Nordgren, Y. Luo, H. Agren, J.E. Sundgren, Appl. Phys. Lett. 79 (2001) 4348–4350.
[92] X. Li, W.J. Hua, J.H. Guo, Y. Li, J. Phys. Chem. C 119 (2015) 16660–16666.
[93] L. Aurelien, R.B.M. Andres, C.C. Jean, Nano Lett. 13 (2013) 1446–1450.
[94] H. Li, J. He, S.J. Li, P.F.T. Anthony, Biosen. Bioelectron. 43 (2013) 25–29.
[95] B.P. Vinayan, R. Nagar, N. Rajalakshmi, S. Ramaprabhu, Adv. Funct. Mater. 22 (2012) 3519–3526.
[96] X. Wang, X.Q. Cao, L. Bourgeois, H. Guan, S.M. Chen, Y.T. Zhong, D.M. Tang, H.Q. Li, T.Y. Zhai, L. Li, Y. Bando, D. Golbery, Adv. Funct. Mater. 22 (2012) 2682–2690.
[97] Z.Y. Ji, X. Shen, M.Z. Li, H. Zhou, G.X. Zhu, K.M. Chen, Nanotechnol. 24 (2013) 115603.
[98] L.B. Ma, X.P. Shen, G.X. Zhu, Z.Y. Ji, H. Zhou, Carbon 77 (2014) 255–265.
[99] S.Y. Wang, D.S. Yu, L.M. Dai, D.W. Chang, J.B. Baek, ACS Nano 5 (2011) 6202–6209.
[100] E.K. Rideal, W.M. Wright, J. Electrochem. Soc. 128 (1926) 1813–1815.
[101] H.B. Wang, T. Maiyalagan, X. Wang, ACS Catal. 2 (2012) 781–794.
[102] K.A. Kurak, A.B. Anderson, J. Phys. Chem. C 113 (2009) 6730–6734.
[103] L.P. Zhang, Z.H. Xia, J. Phys. Chem. C 115 (2011) 11170–11176.
[104] L. Yu, X.L. Pan, X.M. Cao, P. Hu, X.H. Bao, J. Catal. 282 (2011) 183–190.
[105] H.B. Yang, J.W. Miao, S.F. Hung, J.Z. Chen, H.B. Tao, X.Z. Wang, L.P. Zhang, R. Chen, J.J. Gao, H.M. Chen, L.M. Dai, B. Liu, Sci. Adv. 2 (2016) e1501122.
[106] Y. Zhao, C.G. Hu, Y. Hu, H.H. Cheng, G.Q. Shi, L.T. Qu, Angew. Chem. Int. Ed. 51 (2012) 11371–11375.
[107] I.Y. Jeon, D.S. Yu, S.Y. Bae, H.J. Choi, D.W. Chang, L.M. Dai, J.B. Baek, Chem. Mater. 23 (2011) 3987–3992.
[108] B.J. Landi, M.J. Ganter, C.D. Cress, R.A. DiLeo, R.P. Raffaelle, Energy Environ. Sci. 2 (2009) 638–654.
[109] H.L. Lu, R.P. Chen, Y. Hu, X.Q. Wang, Y.R. Wang, L.B. Ma, G.Y. Zhu, T. Chen, Z.X. Tie, Z. Jin, J. Liu, Nanoscale 9 (2017) 1972–1977.
[110] H.L. Lv, R.P. Chen, X.Q. Wang, Y. Hu, Y.R. Wang, T. Chen, L.B. Ma, G.Y. Zhu, J. Liang, Z.X. Tie, J. Liu, Z. Jin, ACS Appl. Mater. Interfaces 9 (2017) 25232–25238.
[111] P. Guo, H.H. Song, X.H. Chen, Electrochem. Commun. 11 (2009) 1320–1324.
[112] N. Kurita, Carbon 38 (2000) 65–75.
[113] L.S. Panchakarla, K.S. Subrahmanyam, S.K. Saha, A. Govindaraj, H.R. Krishnamurthy, U.V. Waghmare, C.N.R. Rao, Adv. Mater. 11 (2009) 4726–4730.
[114] D.B. Xiong, X.F. Li, Z.M. Bai, H. Shan, L.L. Fan, C.X. Wu, D.J. Li, S.G. Lu, ACS Appl. Mater. Interfaces 9 (2017) 10643–10651.
[115] Y.S. Huang, D.Q. Wu, A. Dianat, M. Bobeth, T. Huang, Y.Y. Mai, F. Zhang, G. Cuniberti, X.L. Feng, J. Mater. Chem. A 5 (2017) 1588–1594.

[116] W.Y. Yuan, L.F. Cheng, Y.Z. Zhang, Y.Q. Li, X.H. Guo, H. Wu, L.X. Zheng, Ceram. Int. 43 (2017) 11563–11568.
[117] X.Y. Zhou, S.M. Chen, J. Yang, T. Bai, Y.P. Ren, H.Y. Tian, ACS Appl. Mater. Interfaces 9 (2017) 14309–14318.
[118] C.M. Yang, Y.Q. Qing, K. An, Z.F. Zhang, L.S. Wang, C.S. Liu, Mater. Chem. Phys. 195 (2017) 149–156.
[119] L.Y. Qi, Y.L. Xin, Z.C. Zuo, C.K. Yang, K. Wu, B. Wu, H.H. Zhou, ACS Appl. Mater. Interfaces 8 (2017) 17245–17252.
[120] S. Li, P. Xue, C. Lai, J.X. Qiu, M. Ling, S.Q. Zhang, Electrochim. Acta 180 (2015) 112–119.
[121] J.L. Li, R.H. Li, C. Bulin, R.G. Xing, B.W. Zhang, Int. J. Electrochem. Sci. 12 (2017) 4164–4172.
[122] X.L. Ge, Z.Q. Li, L.W. Yin, Nano Energy 32 (2017) 117–124.
[123] M.D. Slater, D. Kim, E. Lee, C.S. Johnson, Adv. Funct. Mater. 23 (2013) 947–958.
[124] H.W. Lee, H.S. Moon, J. Hur, I.T. Kim, M.S. Park, J.M. Yun, K.H. Kim, S.G. Lee, Carbon 119 (2017) 492–501.
[125] G.Y. Ma, K.S. Huang, Q.C. Zhuang, Z.C. Ju, Mater. Lett. 174 (2016) 221–225.
[126] H. Liu, M.Q. Jia, B. Cao, R.J. Chen, X.Y. Lv, R.J. Tang, F. Wu, B. Xu, J. Power Sources 310 (2016) 195–201.
[127] J.T. Xu, M. Wang, N.P. Wickramaratne, M.J. Jaroniec, S.X. Dou, L.M. Dai, Adv. Mater. 27 (2015) 2042–2048.
[128] J. Zhang, C. Li, Z.K. Peng, Y.S. Liu, J.M. Zhang, Z.Y. Liu, D. Li, Sci. Rep. 7 (2017) 4886.
[129] C. Zhang, X. Wang, Q.F. Liang, X.Z. Liu, Q.H. Weng, J.W. Liu, Y.J. Yang, Z.H. Dai, K.J. Ding, Y. Bando, J. Tang, D. Golberg, Nano Lett. 16 (2016) 2054–2060.
[130] H.X. Liu, Y. Guo, Solid State Ion. 307 (2017) 65–72.
[131] G.Z. Wang, J.M. Feng, L. Dong, L.F. Li, D.J. Li, Appl. Surf. Sci. 396 (2017) 260–277.
[132] D. Zhou, X.G. Li, L.Z. Fan, Y.H. Deng, Electrochim. Acta 230 (2017) 212–221.
[133] C. Liu, F. Li, L.P. Ma, H.M. Cheng, Adv. Mater. 22 (2010) E28–E62.
[134] P. Simon, Y. Gogotsi, Nat. Mater. 7 (2008) 845–854.
[135] D.H. Guan, Z. Gao, W.L. Yang, J. Wang, Y. Yuan, B. Wang, M.L. Zhang, L.H. Liu, Mater. Sci. Eng. B 178 (2013) 736–743.
[136] W.H. Shi, J.X. Zhu, D.H. Sim, Y.Y. Tay, Z.Y. Lu, X.J. Zhang, Y. Sharma, M. Srinivasan, H. Zhang, H.H. Hng, Q.Y. Yan, J. Mater. Chem. 21 (2011) 3422–3427.
[137] J.W. Lee, J.M. Ko, J.D. Kim, Electrochim. Acta 85 (2012) 459–466.
[138] B. You, L.L. Wang, L. Yao, J. Yang, Chem. Commun. 49 (2013) 5016–5018.
[139] D.W. Chang, E.K. Lee, E.Y. Park, H. Yu, H.J. Choi, I.Y. Jeon, G.J. Sohn, D.B. Shin, N. Park, J.H. Oh, L.M. Dai, J.B. Baek, J. Am. Chem. Soc. 135 (2013) 8981–8988.
[140] S.Y. Wang, X.S. Zhao, T. Cochell, A. Manthiram, J. Phys. Chem. Lett. 3 (2013) 2164–2167.